Inorg. Chem. **2006**, *45*, 1828–1838

Solid-State ^{23}Na and ^{7}Li NMR Investigations of Sodium- and Lithium-Reduced Mesoporous Titanium Oxides

Andy Y. H. Lo,[†] Robert W. Schurko,*[,†] Melissa Vettraino,[†] Boris O. Skadtchenko,[†] Michel Trudeau,[‡] and David M. Antonelli*[,†]

Department of Chemistry and Biochemistry, University of Windsor, 401 Sunset Avenue, Windsor, Ontario N9B-3P4, Canada, and Emerging Technologies, Hydro-Québec Research Institute, 1800 Boul. Lionel-Boulet, Varennes, Quebec J3X 1S1, Canada

Received September 26, 2005

Mesoporous titanium oxide synthesized using a dodecylamine template was treated with 0.2, 0.6, and 1.0 equiv of Li– or Na–naphthalene. The composite materials were characterized by nitrogen adsorption, powder X-ray diffraction, X-ray photoelectron spectroscopy, elemental analysis, thermogravimetric analysis, and solid-state ^{23}Na and ^{7}Li NMR spectroscopy. In all cases the wormhole mesoporosity was retained as evidenced by BET surface areas from 400 to 700 m^2/g, Horvath–Kawazoe pore sizes in the 20 Å range, and a lack of hysteresis in the nitrogen adsorption isotherms. Variable-temperature conductivity studies show that the Li-reduced materials are semiconductors, with conductivity values 3 orders of magnitude higher than those of the Na-reduced materials. Electrochemical measurements demonstrate reversible intercalation/deintercalation of Li^+ ions into pristine mesoporous Ti oxides with good cycling capacity. Solid-state ^{23}Na NMR reveals two distinct Na environments: one corresponding to sodium ions in the mesoporous channels and the other corresponding to sodium ions intercalated into the metal framework. ^{23}Na NMR spectra also indicate that the relative population of the framework site increases with increased reduction levels. Solid-state ^{7}Li NMR spectra display a single broad resonance, which increases in breadth with increased reduction levels, though individual resonances inferring the presence of channel and framework Li species are not resolved. Comparisons of the lithium chemical shifts with published values suggests an "anatase-like structure" with no long-range order in the least-reduced samples but a "lithium titanate-like structure" with no long-range order in the higher reduced materials.

Introduction

The design and synthesis of new materials for high-density power sources is one of the most challenging areas of materials science. To meet increasingly strict environmental and performance demands, new battery materials must be developed with superior durability, recharge ability, and current-delivery properties. Dry lithium batteries offer several advantages over wet batteries but are more difficult to design and optimize because the inorganic support material must meet several competing demands.[1−5] To maximize energy output, the cathode must possess a large enough potential difference with respect to the anode. The materials must also be structurally stable through a wide range of Li reduction levels, possess a high capacity per unit weight for maximum Li storage, allow fast diffusion for the Li ions, and allow smooth electron flow to all contact points in the cell. Because of their superior ion and electron transport properties and Li capacity, many high-surface-area porous composite gels have been used as alternatives to the standard layered materials.[6,7] While periodic mesoporous silicas possess high surface area and controlled mesoporosity,[8−12] they do not

* To whom correspondence may be addressed. E-mail: rschurko@uwindsor.ca (R.W.S.), danton@uwindsor.ca (D.M.A.).
[†] University of Windsor.
[‡] Hydro-Québec Research Institute.

(1) Jacobsen, A. *Solid State Chemistry Compounds*; Oxford Science: Oxford, 1992.
(2) Armstrong, A. R.; Bruce, P. G. *Nature* **1996**, *381*, 499.
(3) Huang, H.; Yin, S. C.; Nazar, L. F. *Electrochem. Solid State Lett.* **2001**, *4*, A170.
(4) Yang, S. F.; Song, Y. N.; Zavalij, P. Y.; Whittingham, M. S. *Electrochem. Commun.* **2002**, *4*, 239.
(5) Dong, W.; Rolison, D. R.; Dunn, B. *Electrochem. Solid State Lett.* **2000**, *3*, 457.
(6) Miller, J. M.; Dunn, B. *Langmuir* **1999**, *15*, 799.
(7) Rolison, D. R.; Dunn, B. *J. Mater. Chem.* **2001**, *11*, 963.
(8) Kresge, C. T.; Leonowicz, M. E.; Roth, W. J.; Vartuli, J. C.; Beck, J. S. *Nature* **1992**, *359*, 710.

10.1021/ic051654h CCC: $33.50
Published on Web 01/28/2006

have the flexible oxidation states required for electrochemical applications offered by mesoporous transition metal oxides.[13−20] Recent advances in our group demonstrated that mesoporous Ti, Nb, and Ta oxides could be reduced with up to 1 equiv of alkali metal while still retaining their pore structure.[21] These reduced materials possess surface areas of 400−1000 m^2/g and pore sizes from 20 to 30 Å. The ability to control metal−insulator transitions, by impregnation of the periodic pore structure with redox-active dopants such as organometallic sandwich complexes[22−27] or alkali fullerides,[28,29] makes these mesoporous oxides unique from the standpoint of ion battery applications. In previous work, room-temperature electron transport measurements showed that mesoporous Ti oxide intercalated with 1.0 equiv of Li is semiconducting while all other alkali-reduced mesoporous Nb and Ta oxides are insulating, possibly because of Anderson localization of the electrons in disordered sites.[29] Electrochemical studies showed that mesoporous Nb and Ta oxides behave as capacitors, while mesoporous Ti oxide possesses fully reversible redox behavior.[23] This suggests that mesoporous Ti oxide may be an attractive candidate for use as an anode material, with its high surface area and controlled mesoporosity providing possible transport advantages over standard layered materials such as lithium titanate.[1]

Very little is known about the local structure in the walls of mesoporous Ti oxides, because powder X-ray diffraction (XRD) studies show no reflections apart from that due to the mesoporosity at about $d = 32$ Å. Previous solid-state ^{23}Na, ^{7}Li, and ^{87}Rb NMR studies of mesoporous Ta oxides doped with alkali A_3C_{60} fullerides (A = Na, Li, Rb) allowed for the identification of several different alkali metal/mesostructure sites, and chart the dependence of each site population with the alkali reduction level.[30−32] In this study, solid-state ^{23}Na and ^{7}Li NMR are used as structural probes to elucidate the coordination environment of the sodium and lithium cations in the walls of the Ti oxide substrate at various reduction levels. Variable-temperature (VT) measurements of longitudinal and transverse relaxation time constants, T_1 and T_2, are used to examine the mobility of these species. These NMR studies may also unveil indirect information on the structure of the walls of the mesoporous Ti oxide that cannot be revealed by X-ray photoelectron spectroscopy (XPS) or XRD measurements.

Experimental Section

Materials and Synthesis. All chemicals were obtained from Aldrich, unless otherwise stated. Samples of mesoporous titanium oxide were either obtained from Alfa-Aesar and used without further purification or synthesized according to the literature.[33−35] Trimethylsilyl chloride was distilled over calcium hydride. The mesoporous titanium oxide was dried at 200 °C overnight under vacuum and then stirred with excess trimethylsilyl chloride in dry ether for 12 h under nitrogen. A total of 0.2, 0.6, or 1.0 equiv of Li− or Na−naphthalene was added to a suspension of mesoporous titanium oxide in dry tetrahydrofuran (THF), as calculated on the basis of % Ti that determined from the inductively coupled plasma (ICP) elemental analysis data. Typically, the mesoporous titanium oxide samples contain about 38% Ti by weight after treatment with trimethylsilyl chloride. For example, 0.055 g of Li metal represents 1.0 molar equiv with respect to 1.0 g of the titanium oxide. The mesoporous solid immediately went from a light fawn color (pure mesoporous Ti oxide) to a deep gray-black or dark blue after treatments of Na− and Li−naphthalene, respectively. After several hours of additional stirring to ensure complete reduction, the dark solid was collected by suction filtration and washed several times with THF. The material was finally dried in vacuo at 10^{-3} Torr on a Schlenk line, until all condensable and volatile substances had been removed.

Characterization of Materials. Nitrogen adsorption/desorption data were collected on a Micromeritics ASAP 2010 analyzer. Powder XRD patterns (Cu Kα) were recorded in a sealed glass capillary on a Siemens D-500 diffractometer. All XPS experiments were conducted on a Physical Electronics PHI-5500 spectrometer with charge neutralization. Resonances in XPS spectra were referenced to the carbon C-(C, H) peak at 284.8 eV. Room-temperature conductivity measurements were recorded on a Jandel four-point universal probe head combined with a Jandel resistivity unit. The equations used for calculating the resistivity were as follows: for pellets of less than 0.1 mm thickness, $\rho = [\pi V/(I \log n^2)]t$, and for pellets of less than 0.5 mm thickness, $\rho = 2\pi SV/I$, where $\rho =$ resistivity, $\pi/(\log n^2) =$ sheet resistivity, $V =$ voltage, $I =$ current, $t =$ thickness of the pellet, and $S =$ the spacing of the probes (0.1 cm). VT conductivity and magnetic measurements were conducted on a Quantum Design superconducting quantum interference device (SQUID) magnetometer equipped with the MPMS system and a 5 T magnet. Four copper wires were affixed to pressed pellets of the mesoporous composites with silver paste and then coated with a

(9) Huo, Q. S.; Margolese, D. I.; Ciesla, U.; Demuth, D. G.; Feng, P. Y.; Gier, T. E.; Sieger, P.; Firouzi, A.; Chmelka, B. F.; Schuth, F.; Stucky, G. D. *Chem. Mater.* **1994**, *6*, 1176.
(10) Chen, C. Y.; Burkett, S. L.; Li, H. X.; Davis, M. E. *Microporous Mater.* **1993**, *2*, 27.
(11) Tanev, P. T.; Chibwe, M.; Pinnavaia, T. J. *Nature* **1994**, *368*, 321.
(12) Behrens, P. *Angew. Chem., Int. Ed. Engl.* **1996**, *35*, 515.
(13) Antonelli, D. M.; Ying, J. Y. *Angew. Chem., Int. Ed. Engl.* **1995**, *34*, 2014.
(14) Antonelli, D. M.; Ying, J. Y. *Angew. Chem., Int. Ed. Engl.* **1996**, *35*, 426.
(15) Reddy, J. S.; Sayari, A. *Catal. Lett.* **1996**, *38*, 219.
(16) Antonelli, D. M. *Adv. Mater.* **1999**, *11*, 487.
(17) Tian, Z. R.; Tong, W.; Wang, J. Y.; Duan, N. G.; Krishnan, V. V.; Suib, S. L. *Science* **1997**, *276*, 926.
(18) Antonelli, D. M.; Trudeau, M. *Angew. Chem., Int. Ed.* **1999**, *38*, 1471.
(19) Ciesla, U.; Schacht, S.; Stucky, G. D.; Unger, K. K.; Schuth, F. *Angew. Chem., Int. Ed. Engl.* **1996**, *35*, 541.
(20) Mamak, M.; Coombs, N.; Ozin, G. *J. Am. Chem. Soc.* **2000**, *122*, 8932.
(21) Vettraino, M.; Trudeau, M. L.; Antonelli, D. M. *Adv. Mater.* **2000**, *12*, 337.
(22) He, X.; Antonelli, D. *Angew. Chem., Int. Ed.* **2001**, *41*, 214.
(23) Vettraino, M.; Trudeau, M.; Antonelli, D. M. *Inorg. Chem.* **2001**, *40*, 2088.
(24) He, X.; Trudeau, M.; Antonelli, D. *Adv. Mater.* **2000**, *12*, 1036.
(25) Murray, S.; Trudeau, M.; Antonelli, D. M. *Inorg. Chem.* **2000**, *39*, 5901.
(26) Murray, S.; Trudeau, M.; Antonelli, D. M. *Adv. Mater.* **2000**, *12*, 1339.
(27) Vettraino, M.; Trudeau, M.; Lo, A. Y. H.; Schurko, R. W.; Antonelli, D. *J. Am. Chem. Soc.* **2002**, *124*, 9567.
(28) Ye, B.; Trudeau, M.; Antonelli, D. *Adv. Mater.* **2001**, *13*, 29.
(29) Ye, B.; Trudeau, M. L.; Antonelli, D. M. *Adv. Mater.* **2001**, *13*, 561.
(30) Skadtchenko, B. O.; Trudeau, M.; Schurko, R. W.; Willans, M. J.; Antonelli, D. *Adv. Funct. Mater.* **2003**, *13*, 671.
(31) Skadtchenko, B. O.; Trudeau, M.; Kwon, C. W.; Dunn, B.; Antonelli, D. *Chem. Mater.* **2004**, *16*, 2886.
(32) Skadtchenko, B. O.; Trudeau, M.; Schurko, R. W.; Lo, A. Y. H.; Antonelli, D. M. *Chem. Mater.* **2005**, *17*, 1467.
(33) Antonelli, D. M. *Microporous Mesoporous Mater.* **1999**, *30*, 315.
(34) Wang, Y. Q.; Tang, X. H.; Yin, L. X.; Huang, W. P.; Hacohen, Y. R.; Gedanken, A. *Adv. Mater.* **2000**, *12*, 1183.
(35) Yoshitake, H.; Sugihara, T.; Tatsumi, T. *Chem. Mater.* **2002**, *14*, 1023.

layer of epoxy for protection from the air. Elemental analysis data were acquired under an inert atmosphere by Galbraith Laboratories, 2323 Sycamore Drive, Knoxville, TN 37921-1700. Metal analysis was conducted by ICP techniques. Thermogravimetric analysis (TGA), to determine water and organic content as well as overall stability, was done on a Perkin-Elmer TGA 7 analyzer using loose powder spread on a platinum pan, typically from 30 to 500 °C at a rate of 5 °C/min in oxygen gas.

Electrochemistry. Electrochemical measurements were performed using bag cells at room temperature with a pure lithium anode, using a Mac Pile II instrument for cycling at 0.2 mA cm^{-2} between 3.6 and 1.0 V. The cathode was constructed by mixing the mesoporous materials with carbon black (City Services Co.) and Teflon powder (Dupont) in a 80:10:10 ratio. The mixture was hot pressed at 180 °C into a stainless steel Exmet grid. The electrolyte used was $LiPF_6$ in a mixture of dimethyl carbonate and ethyl carbonate (LP30 from EM Industries).

Solid-State NMR. Solid-state ^{23}Na and ^{7}Li NMR experiments were performed on a Varian Infinity Plus 9.4 T wide-bore NMR spectrometer operating at $\nu_0 = 105.7$ and 155.35 MHz, respectively, using a Varian/Chemagnetics 4 mm HX magic-angle spinning (MAS) probe. All samples were carefully powdered under an inert atmosphere and were tightly packed into 4 mm o.d. zirconium oxide rotors which were sealed with airtight Teflon spacer and caps at both ends. ^{23}Na NMR spectra were referenced with respect to a 1.0 M NaCl solution with $\delta_{iso}(^{23}Na) = 0.0$ ppm, and ^{7}Li NMR spectra were referenced with respect to a 1.0 M LiCl solution with $\delta_{iso}(^{7}Li) = 0.0$ ppm. To avoid baseline distortions which occur while using Bloch decay experiments to acquire broad powder patterns, rotor-synchronized ^{23}Na and ^{7}Li MAS NMR experiments were conducted using a Hahn-echo pulse sequence of the form $(\pi/2)_x-\tau-(\pi)_y-\tau-$acquire, with spinning speeds of about $\nu_{rot} = 8.0$ kHz. The central-transition (CT) selective $\pi/2$ pulse width used in the ^{23}Na NMR experiments was 3.75 μs with a radio frequency field of $\nu_1(^{23}Na) = 33.3$ kHz. For ^{7}Li NMR experiments, the CT selective $\pi/2$ pulse was 2.5 μs and $\nu_1(^{7}Li) = 50.0$ kHz. Between 16 and 64 transients were collected in each experiment, with calibrated recycle times of 7.0 s for ^{23}Na and 4.0 s for ^{7}Li. VT ^{23}Na MAS NMR experiments were also performed from +150 °C to −100 °C on the 1.0 equiv sample.

Measurements of longitudinal (T_1) and transverse (T_2) relaxation time constants were conducted on the 1.0 equiv sample from +100 to −70 °C. Saturation recovery experiments were conducted for the measurement of T_1 time constants, where about 100 $\pi/2$ pulses with 10 μs delays were applied to saturate the magnetization prior to detection. For T_2 relaxation measurements, Hahn echo pulse sequences with linearly incremented interpulse delays were applied. Extractions of T_1 and T_2 time constants were accomplished by fitting the T_1 and T_2 curves, respectively, using the functions $y(\tau) = A_f[1 - \exp(-\tau/T_{1f})] + A_s[1 - \exp(-\tau/T_{1s})]$ and $y(\tau) = B_f \exp(-\tau/T_{2f}) + B_s \exp(-\tau/T_{2s})$, where the subscripts "f" and "s" refer to fast and slow, respectively.

Results and Discussion

TGA was conducted in an oxygen atmosphere on mesoporous Ti oxide (Figure 1). A steady loss of weight with increasing temperature is observed, which corresponds to the loss of water from the structure. Up to 26% of the total weight is lost by 500 °C, with 21% of this coming by the end of the sharp dip at 200 °C, after which little or no water is removed up to 300 °C. The weight loss between 300 °C and 500 °C, a temperature range over which mesoporous titanium oxide collapses, amounts to only 5% of the overall mass and is likely related to condensation of neighboring hydroxyl groups as opposed to loss of physisorbed water. This water loss due to condensation and densification of the walls is observed for samples of mesoporous silica on heating.[10] Thus, to remove excess moisture from the samples that may interfere with alkali reduction by producing hydroxide and H_2, all materials were dried at 200 °C overnight under vacuum. Capping of leftover hydroxyl groups on the surface, which may also interfere with reduction, was accomplished as previously reported by stirring with an excess of trimethylsilyl chloride in dry diethyl ether for 12 h under nitrogen.[31]

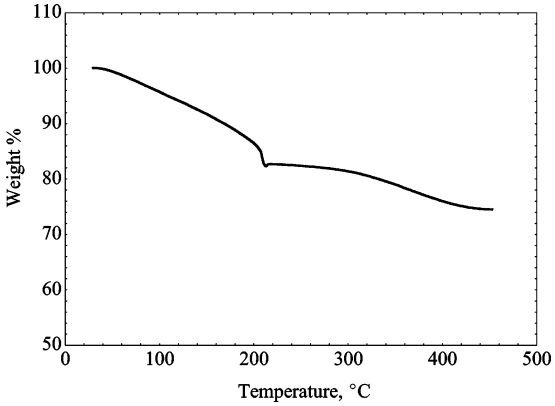

Figure 1. TGA of pristine mesoporous Ti oxide.

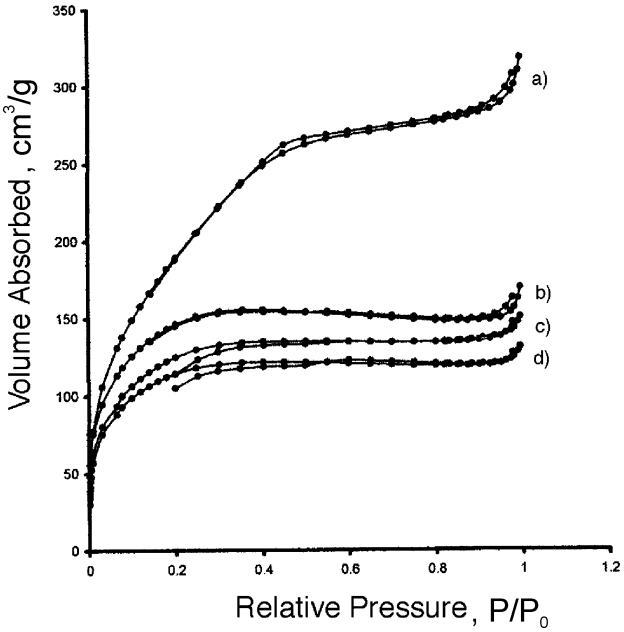

Figure 2. Nitrogen adsorption and desorption isotherms of (a) mesoporous titanium oxide, and mesoporous titanium oxide reduced with (b) 0.2, (c) 0.6, and (d) 1.0 equiv of Li−naphthalene.

Nitrogen adsorption and desorption isotherms of mesoporous titanium oxide progressively reduced with Li−naphthalene or Na−naphthalene, respectively, are shown in Figures 2 and 3. In all cases an isotherm between type I and type IV is obtained, indicating retention of mesoporosity upon reduction. The intermediate type I/IV isotherm is commonly observed in mesoporous transition metal oxides

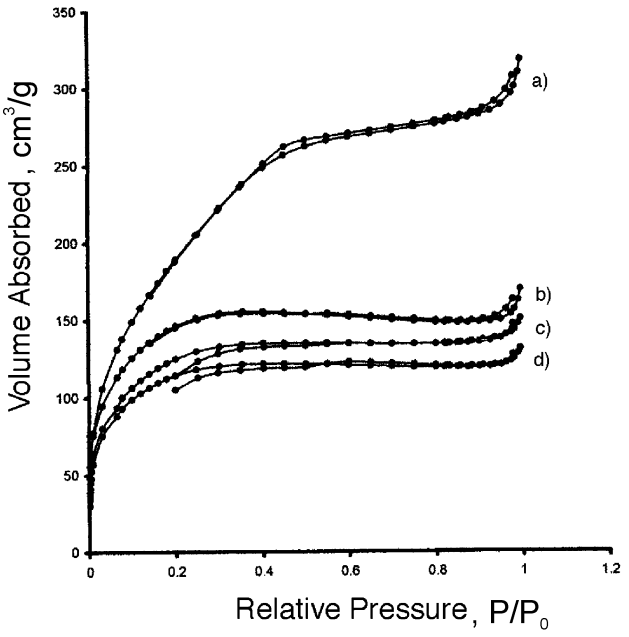

Figure 3. Nitrogen adsorption and desorption isotherms of (a) mesoporous titanium oxide, and mesoporous titanium oxide reduced with (b) 0.2, (c) 0.6, and (d) 1.0 equiv of Na−naphthalene.

Table 1. Nitrogen Adsorption Data as a Function of the Li and Na Reduction Levels in Mesoporous Ti Oxide

	BET surface area (m^2/g)	HK pore size (Å)	HK pore volume (cm^3/g)
TiTMSl	723	20.6	0.479
0.2 LiTi	550	20.5	0.291
0.6 LiTi	454	20.6	0.167
1.0 LiTi	320	19.7	0.091
0.2 NaTi	530	19.8	0.268
0.6 NaTi	415	20.5	0.118
1.0 NaTi	356	20.6	0.087

synthesized with a dodecylamine template because the 20 Å pore sizes are on the lower threshold of the mesoporous regime.[23] The BET surface areas, HK (Horvath−Kawazoe) pore sizes, and HK pore volumes are summarized in Table 1. The gradual decrease in per-gram surface area on increase in alkali metal intercalation is consistent with the increased density of the material upon introduction of the alkali metal to the framework, although some loss of structure may also be occurring. This is supported by the loss in long-range order observed in the powder XRD experiments on these samples, which are similar to those acquired in previous studies on these materials.[23] Mesoporous Nb and Ta oxides typically retain their structure upon reduction, even by alkali−naphthalene reagents, while mesoporous Ti oxides retain their mesoporosity but lose their XRD patterns upon reduction in almost all cases. The exception to this is reduction by bis(toluene)titanium which is believed to act as a Ti atom donor to the walls of the mesostructure.[27] In this instance, addition of Ti atoms to weaker areas of the mesostructure may actually improve thermal stability of the titanium oxide framework.

XPS Experiments. XPS spectra of the mesoporous Ti oxide reduced with 0.2, 0.6, and 1.0 equiv of lithium showed a gradual movement to lower binding energies for the Ti

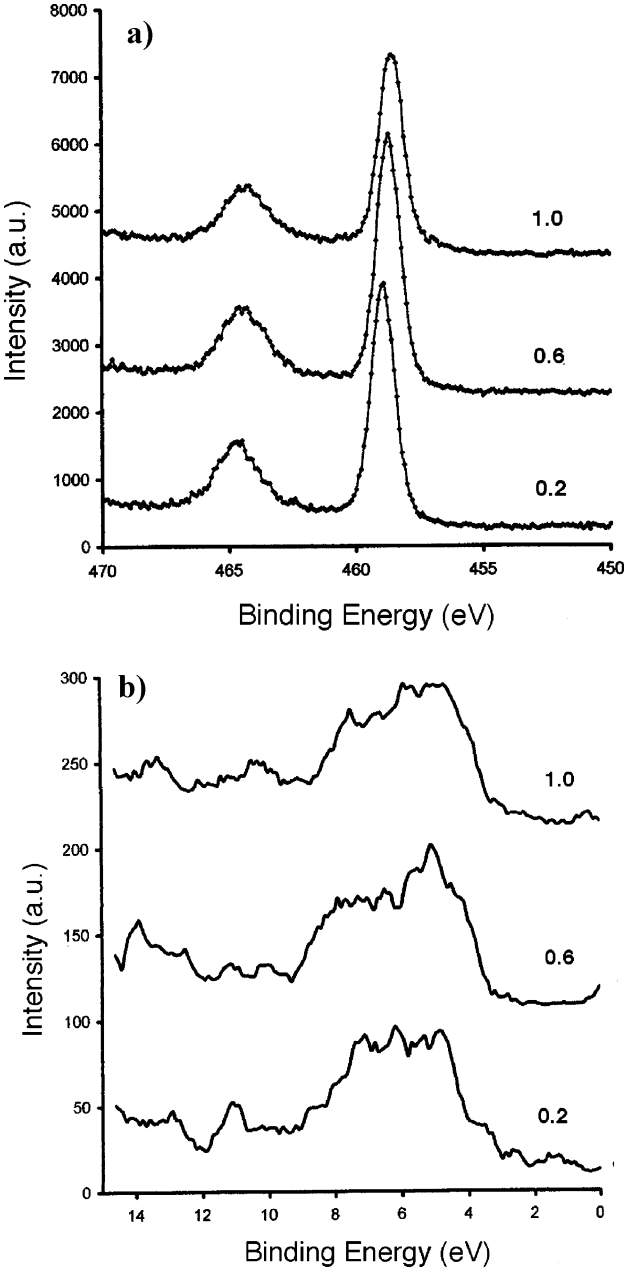

Figure 4. XPS spectra showing (a) the Ti $2p_{1/2}$ and $2p_{3/2}$ regions, and (b) the region near the Fermi level for reduced mesoporous titanium oxide with 0.2, 0.6, and 1.0 equiv of Li−naphthalene.

$2p_{1/2}$ and $2p_{3/2}$ emissions (Figure 4a), with values of 464.5 and 458.9 eV for the least-reduced sample, 464.3 and 458.7 eV for the intermediate one, and 464.2 and 458.5 eV for the most-reduced sample. This same trend was observed in the sodium-intercalated Ti oxide materials (Figure 5a), which showed Ti $2p_{1/2}$ and $2p_{3/2}$ binding energies of 464.5 and 458.8 eV for the 0.2 equiv sample and 464.2 and 458.4 eV for the 0.6 equiv sample, down to 463.8 and 458.0 eV for the 1.0 equiv sample. This decrease in binding energies in both alkali-reduced samples is consistent with increasing levels of reduction of the porous framework and lowering of the average oxidation state of the Ti center. The small differences in binding energies between Li- and Na-reduced species have been commented on previously[24] and have been related to more complete charge transfer by Na to the acceptor

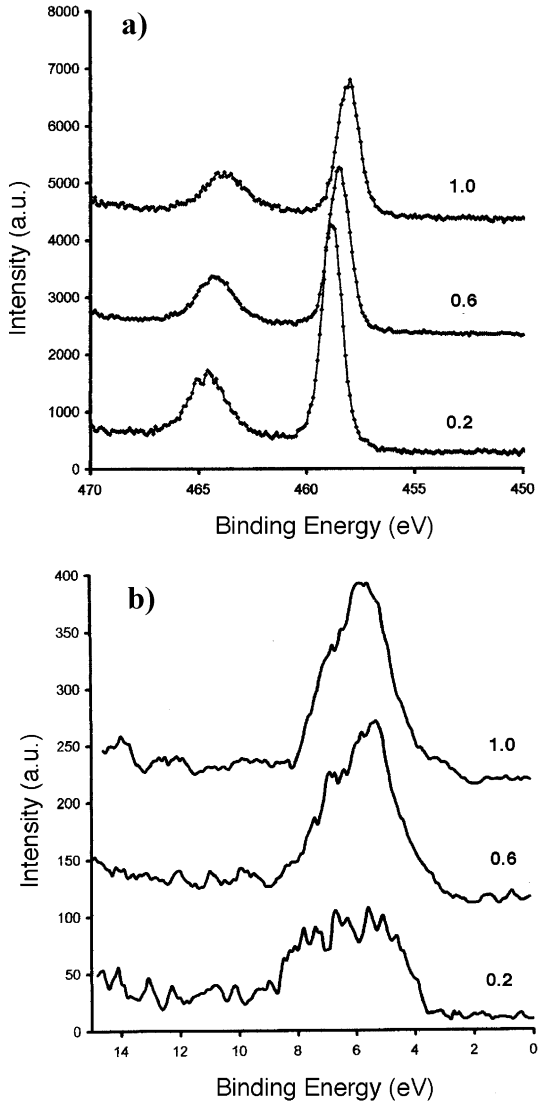

Figure 5. XPS spectra showing (a) the Ti $2p_{1/2}$ and $2p_{3/2}$ regions, and (b) the region near the Fermi level for reduced mesoporous titanium oxide with 0.2, 0.6, and 1.0 equiv of Na−naphthalene.

framework. The region near the Fermi level for the materials reduced with 0.2, 0.6, and 1.0 equiv of Li−naphthalene is shown in Figure 4b. The large emission beginning at about 3.0 eV from the Fermi level can be assigned to the O 2p valence band emission, while there are no clear emissions for the Ti 3d valence electrons expected from reduction of the Ti atoms in the walls of the structure; however, the small humps near the Fermi level in each sample could be attributed to these emissions. The lack of an obvious 3d emission is consistent with very broad states due to the amorphous nature of the walls.[36] Materials reduced with bis(toluene)titanium show a much more prominent emission at the Fermi level because of the metallic nature of the low-valent walls of the structure.[27] The region near the Fermi level for the corresponding Na-reduced materials is shown in Figure 5b, displaying a large peak for the O 2p emission with no second emission near the Fermi level as observed in the Li-reduced materials. There is a small broadening of the O 2p peak accompanied by the emergence of a tail at lower binding energy in the high reduction sample, which may be due to the 3d emission.

Measurements of conductivity as a function of temperature for the material reduced with 1.0 equiv of Li−naphthalene show that this material is a semiconductor, with the conductivity dropping from 5×10^{-4} Ω^{-1} cm^{-1} to 3.0×10^{-7} Ω^{-1} cm^{-1} from room temperature down to −100 °C. Materials reduced with less Li−naphthalene or any amount of Na−naphthalene were insulating in all cases with conductivity values less than 10^{-7} Ω^{-1} cm^{-1}. The drop in conductivity with temperature is consistent with semiconducting rather than metallic behavior. Related alkali-reduced tungsten oxides undergo an Anderson transition from insulating to metallic behavior upon increased alkali impregnation;[36] however, metallic behavior was not observed for any alkali metal-reduced mesoporous Ti oxides. The higher conductivity of the Li-reduced materials over the Na-reduced materials and the difference in sample color (blue vs black) are not understood; however, these characteristics are likely related to subtle differences in electronic structure between the two materials. In contrast, materials reduced with appropriate levels of bis(toluene)titanium show metallic conductivity due to a low-valent Ti oxide coat over the surface of the material.[27]

Electrochemistry. The voltage profile (Figure 6a) is fairly typical of titanium oxides around 1.5 V. Such behavior normally corresponds to reversible insertion of Li^+ ions, and similar profiles were observed in amorphous and mesoporous Ti oxides,[37,38] lithium titanium spinel,[39] anatase,[40] and rutile.[41] Essentially, the reactions correspond to reversible single phase Li_xTiO_y formation, and the charge capacity is retained for several cycles. The charge capacity progressively degrades with each cycling increment and drops significantly after approximately the sixth cycle (Figure 6b); however, the cycling may be improved by optimizing the cell conditions or processing parameters of the materials.[38] These results are similar to previous studies of mesoporous Ta oxides reduced with C_{60}.[31] The loss of charge capacity upon discharge may be related to reduction of Ti−OH groups that could not be capped because they are imbedded too deeply within the walls of the structure.

Solid-State NMR. While XRD provides information on the degree of crystallinity in the mesostructure and XPS studies reveal a wealth of information on the electronic states at the surface, very little is known about the local structure of mesoporous Ti oxide synthesized by the ligand-assisted templating method. An extended X-ray absorption fine structure study on mesoporous Ti oxide synthesized using a

(36) Cheetham, A. K.; Day, P. *Solid State Chemistry Techniques*; Oxford, 1998.

(37) Leroux, F.; Piffard, Y.; Ouvrard, G.; Mansot, J. L.; Guyomard, D. *Chem. Mater.* **1999**, *11*, 2948.

(38) Leroux, F.; Dewar, P. J.; Intissar, M.; Ouvrard, G.; Nazar, L. F. *J. Mater. Chem.* **2002**, *12*, 3245.

(39) Bach, S.; Pereira-Ramos, J. P.; Baffier, N. *J. Mater. Chem.* **1998**, *8*, 251.

(40) Krtil, P.; Fattakhova, D.; Kavan, L.; Burnside, S.; Gratzel, M. *Solid State Ionics* **2000**, *135*, 101.

(41) Kavan, L.; Fattakhova, D.; Krtil, P. *J. Electrochem. Soc.* **1999**, *146*, 1375.

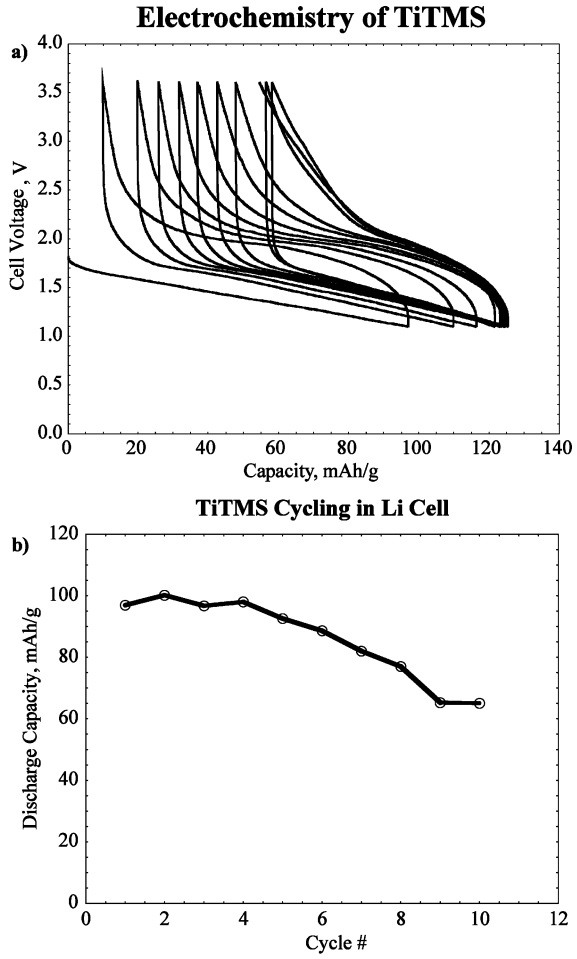

Figure 6. Plots of (a) cell voltage vs capacity at constant current and (b) discharge capacity vs number of cycles for pristine mesoporous Ti oxide. Values on each axis are within 5% error.

dodecylamine template suggests the presence of both 5- and 6-coordinate Ti in the walls;[35] however, there is clearly much more to learn about the wall structure in these materials. Solid-state ^{29}Si NMR is a powerful tool for the study of local structure in mesoporous silicas;[42] however, the walls of the mesoporous metal oxides discussed herein do not contain a receptive spin-1/2 NMR nucleus that can be readily used as a structural probe. ^{47}Ti and ^{49}Ti are quadrupolar nuclei with relatively small quadrupole moments ($Q(^{47}\mathrm{Ti}) = 0.302 \times 10^{-28}$ m^2 and $Q(^{49}\mathrm{Ti}) = 0.247 \times 10^{-28}$ m^2);[43] however, both titanium nuclides have very low NMR frequencies (near 22.5 MHz at 9.4 T) and low natural abundances, complicating the practical consideration of conducting experiments at standard magnetic field strengths. ^{17}O NMR studies are feasible but require isotopic labeling, and they are to be addressed in a separate study. As a means of probing the structure of the walls indirectly, it is possible to conduct NMR experiments on the guest sodium and lithium cations. ^{23}Na and ^{7}Li are half-integer quadrupolar nuclei (both spin 3/2) and are extremely receptive NMR nuclides, possessing reasonably small nuclear quadrupole moments ($Q(^{23}\mathrm{Na}) = 0.104 \times 10^{-28}$ m^2 and $Q(^{7}\mathrm{Li}) = -0.0401 \times 10^{-28}$ m^2),[43] high natural abundances (100 and 92.6%, respectively), and high NMR frequencies. ^{23}Na and ^{7}Li NMR experiments have been applied in many instances to the study of microporous[44−47] and mesoporous solids[30,31,48,49] and are applied in this work as useful probes of the coordination environment at the alkali metals in Na- or Li-reduced mesoporous Ti oxides.

Sodium-23 NMR. ^{23}Na MAS NMR spectra of mesoporous Ti oxide reduced with 0.2, 0.6, and 1.0 equiv of Na−naphthalene are shown in Figure 7. All of the spectra have a sharp resonance near 0 ppm with full widths at half-height (fwhh) of 300 Hz, flanked by spinning sidebands which are indicative of a small quadrupolar interaction. At reduction levels of 0.6 and 1.0 equiv, broad peaks are observed which are centered at about −20 ppm and −15 ppm, with fwhh's of 1200 and 2350 Hz, respectively. Increasing the reduction level also results in a slight shift of the narrow resonance in the high-frequency direction, from 0.37 ppm (0.2 equiv) to 0.52 ppm (0.6 equiv) to 0.71 ppm (1.0 equiv). Deconvolution of the powder patterns, including all of the spinning sidebands associated with the narrow resonance, yields the following relative integrated areas of narrow and broad powder patterns at room temperature: 1:0.02, 1:0.59, and 1:0.91 reduced with 0.2, 0.6, and 1.0 equiv Na−naphthalene, respectively. In corresponding static ^{23}Na NMR experiments, the individual sites are not resolved, a result of increased broadening resulting largely from nonaveraged quadrupolar interactions.

Similar spectra have been reported for buried sodium sites in mesoporous aluminosilicates[49] and for mesoporous metal oxides intercalated with sodium fullerides and reduced with Na−naphthalene.[30] On the basis of these previous assignments, the sharp peaks near 0 ppm can be attributed to sodium cations which are contained within the mesoporous channels, whereas the broader resonances correspond to sodium cations which are confined within the walls of the metal oxide mesostructure. As the reduction level is increased, the augmented intensity of the broad resonance indicates that an increased number of sodium cations are becoming confined within the walls of the mesoporous framework. The broadening of this resonance can potentially result from several sources, including an increased quadrupolar interaction at the ^{23}Na nuclei, an inhomogeneous distribution of chemical shifts and quadrupolar coupling constants due to disorder, ^{23}Na−^{23}Na homonuclear dipolar coupling, and/or homogeneous broadening which arises from environment-dependent transverse relaxation time constants. Acquisition of spectra at a second magnetic field would be

(42) Simonutti, R.; Comotti, A.; Bracco, S.; Sozzani, P. *Chem. Mater.* **2001**, *13*, 771.
(43) Pyykko, P. *Mol. Phys.* **2001**, *99*, 1617.
(44) Grey, C. P.; Poshni, F. I.; Gualtieri, A. F.; Norby, P.; Hanson, J. C.; Corbin, D. R. *J. Am. Chem.* Soc. **1997**, *119*, 1981.
(45) Lim, K. H.; Grey, C. P. *J. Am. Chem. Soc.* **2000**, *122*, 9768.
(46) Engelhardt, G.; Sieger, P.; Felsche, J. *Anal. Chim. Acta* **1993**, *283*, 967.
(47) Feuerstein, M.; Hunger, M.; Engelhardt, G.; Amoureux, J. P. *Solid State Nucl. Magn. Reson.* **1996**, *7*, 95.
(48) Kloetstra, K. R.; vanLaren, M.; vanBekkum, H. *J. Chem. Soc., Faraday Trans.* **1997**, *93*, 1211.
(49) Du, H. B.; Terskikh, V. V.; Ratcliffe, C. I.; Ripmeester, J. A. *J. Am. Chem. Soc.* **2002**, *124*, 4216.

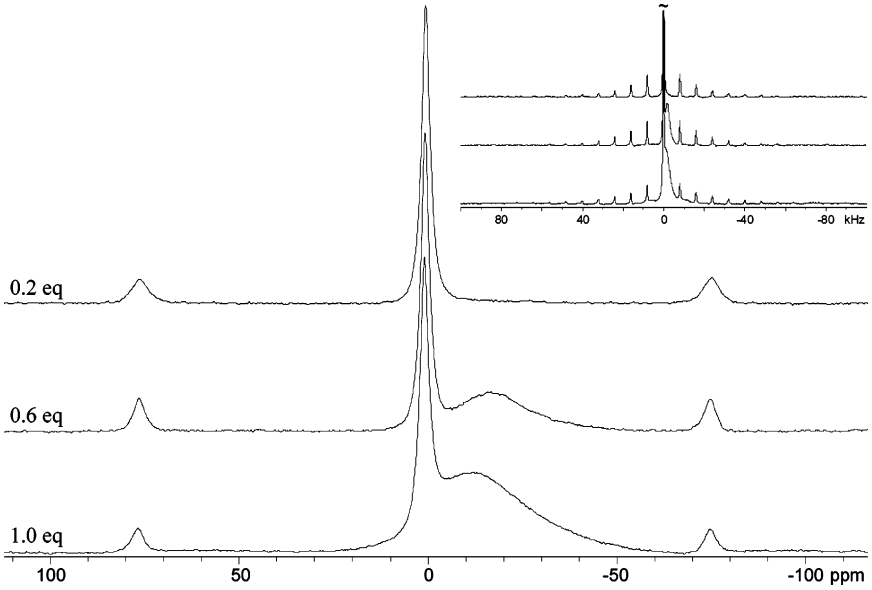

Figure 7. Solid-state ^{23}Na MAS NMR spectra (ν_{rot} = 8 kHz) of mesoporous Ti oxide composite materials reduced with Na−naphthalene. Inset: vertical expansion of corresponding NMR spectra.

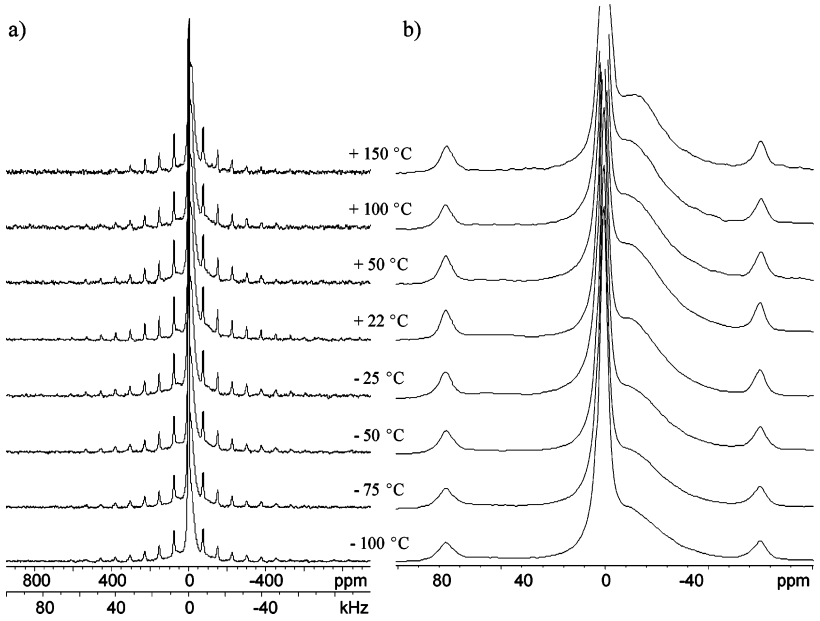

Figure 8. (a) Solid-state VT ^{23}Na MAS NMR spectra (ν_{rot} = 8 kHz) of mesoporous Ti oxide reduced with 1.0 equiv of Na−naphthalene. (b) High-resolution spectra of the isotropic regions.

necessary to absolutely deconvolute the individual contributions from some of these mechanisms, but several factors point to a distribution of large quadrupolar interactions as the main source of peak broadening: (i) the sodium chemical shift range for diamagnetic compounds is relatively small (ca. 120 ppm) and a large distribution of shifts (spanning over ca. 2350 Hz) for chemically similar sites is very unlikely;[50] (ii) MAS speeds of 8 kHz would completely average all ^{23}Na−^{23}Na dipolar couplings, unless individual ^{23}Na nuclei are less than 1 Å apart (i.e., the dipolar coupling constant, R_{DD}(^{23}Na,^{23}Na) = 8.4 kHz at 1.0 Å); and (iii) long-range disorder and a variety of nonspherically symmetric sodium sites in the mesoporous walls are consistent with a distribution of large quadrupolar interactions (as well as the absence of spinning sidebands for the broad resonance). Issues of contributions to peak widths from relaxation phenomena are addressed later in this discussion.

VT ^{23}Na MAS NMR experiments were conducted on the sample with highest reduction level (1.0 equiv of Na−naphthalene) to determine if temperature change has an effect on the relative populations of channel and framework sodium cations. The spinning sideband manifold does not change significantly with temperature, indicating a relatively constant quadrupolar interaction and, therefore, a relatively consistent local environment at the sodium cations (Figure 8). In addition, variation in temperature does not seem to have a noticeable effect on the chemical shift of the narrow resonance. However, the center of gravity of the broad resonance

(50) Mason, J. *Multinuclear NMR*; Plenum Press: New York, 1987.

Table 2. ^{23}Na Longitudinal and Transverse (T_1 and T_2)[a,b] Relaxation Time Constants for Sodium Sites in Mesoporous Titanium Oxide Reduced with 1.0 equiv of Na−Naphthalene

	monoexponential		biexponential				
temperature (°C)	A	T_1 (ms)	A_f	T_{1f} (ms)	A_s	T_{1s} (ms)	A_f/A_s[d]
			Channel Na Site				
100	2009 (30)[c]	988 (77)	557 (45)	96 (17)	1501 (43)	1693 (85)	0.37
22	5093 (64)	1176 (72)	1744 (202)	245 (44)	3499 (194)	2198 (163)	0.50
−35	3103 (46)	1813 (110)	1768 (96)	822 (51)	1506 (88)	5172 (414)	1.17
−70	1856 (31)	2026 (133)	1060 (58)	891 (59)	923 (51)	6252 (559)	1.15
			Framework Na Site				
100	842 (3)	26 (1)	N/A [e]	N/A	N/A	N/A	N/A
22	1858 (22)	54 (4)	922 (69)	18 (2)	965 (69)	162 (16)	0.96
−35	1135 (15)	157 (17)	683 (42)	64 (6)	477 (41)	577 (58)	1.43
−70	647 (9)	221 (24)	374 (23)	76 (7)	290 (22)	749 (76)	1.29

	monoexponential		biexponential				
temperature (°C)	B	T_2 (ms)	B_f	T_{2f} (ms)	B_s	T_{2s} (ms)	B_f/B_s[d]
			Channel Na Site				
100	3503 (241)	0.82 (10)	3417 (250)	0.28 (5)	1238 (197)	2.61 (42)	2.76
22	4166 (252)	1.19 (13)	3777 (251)	0.38 (6)	1608 (247)	3.32 (52)	2.35
−70	5484 (335)	1.55 (2)	5213 (212)	0.54 (5)	1705 (186)	6.06 (85)	3.06
			Framework Na Site				
100	1007 (59)	2.23 (25)	908 (30)	0.41 (3)	509 (23)	5.05 (29)	1.78
22	1575 (45)	3.74 (21)	837 (43)	0.98 (9)	958 (46)	6.51 (33)	0.87
−70	2138 (44)	7.37 (35)	724 (38)	1.42 (14)	1634 (42)	10.53 (32)	0.44

[a] Extraction of T_1 time constants was accomplished using the functions $A[1 - \exp(-\tau/T_1)]$ and $A_f[1 - \exp(-\tau/T_{1f})] + A_s[1 - \exp(-\tau/T_{1s})]$ for monoexponential and biexponential fits, respectively. The subscripts "f" and "s" refer to fast and slow, respectively. [b] Extraction of time constants T_2 was accomplished using the functions $B\exp(-\tau/T_1)$ and $B_f\exp(-\tau/T_{2f}) + B_s\exp(-\tau/T_{2s})$ for monoexponential and biexponential fitting, respectively. [c] All error bounds obtained from least-squares fitting are enclosed in parentheses. [d] A_f/A_s and B_f/B_s are the ratios of the weighted contributions of the "fast" and "slow" relaxation mechanisms. [e] Biexponential fit is not reported for this temperature point as a result of lack of convergence in the least-squares fitting software.

corresponding to framework sodium cations shifts very slightly from about −15.0 ppm at +150 °C to about −12.0 ppm at −100 °C. Furthermore, as the temperature changes, there does not seem to be a discernible trend in changing peak widths or integrated areas of both the narrow and the broad powder patterns. Thus, the relative site populations appear to be solely determined by the reduction level, and, hence, site exchange is unlikely to happen. Temperature-dependent relaxation rates may influence the relative intensities of these peaks; however, calibrated spin−echo delays and relaxation times were determined to quantitatively acquire ^{23}Na MAS NMR spectra for the purposes of comparing relative site populations, effectively eliminating relaxation effects as a factor.[51,52]

Measurements of ^{23}Na longitudinal and transverse relaxation time constants were conducted from +100 to −70 °C, to (i) examine the dependence of relaxation times on temperature, (ii) gain insight into the temperature-dependent dynamics of the sodium cations, and (iii) estimate contributions from transverse relaxation to the widths of the observed resonances. Relaxation measurements were only conducted on the sample with the highest reduction level with coarse steps in temperature, due to the relatively long experimental times associated with acquiring data at each temperature point. Relaxation curves at individual temperatures were fit using both monoexponential and biexponential functions (Table 2). The biexponential fits involve two time constants, for example, T_{1f} and T_{1s}, which represent "fast" and "slow" relaxation mechanisms, respectively. Contributions from multiple relaxation mechanisms are well-known for a variety of NMR nuclei undergoing slow restricted motions in solid materials.[53] For instance, detailed measurements of ^{23}Na relaxation time constants of Na species in zeolites NaX and NaY have previously been reported, where relaxation data were fit with similar biexponential functions.[54,55] Generally speaking, better data fits are obtained herein for biexponential functions, especially for the narrow peak corresponding to the channel Na cations (Figure 9a and Supporting Information). Both mono- and biexponential fits follow similar trends with changes in temperature; thus, for simplicity, reference will be made to the constants from monoexponential fits, unless otherwise noted.

At all temperatures, the T_1 time constants of the channel species are on the order of 1−2 s and are approximately 1 to 2 orders of magnitude larger than those of the framework species. If the quadrupolar relaxation mechanism is dominant, this supports the hypothesis that there are substantially larger quadrupolar interactions at the framework sodium sites. At 100 and 22 °C, the T_1 values do not change much for either site; however, as the temperature is dropped to −70 °C, the T_1 increases substantially at each site. The increase in T_1 with decreasing temperature at both sites is consistent with an increased correlation time and increasingly restricted motion, and does not arise from any significant changes in the magnitude of the quadrupolar interaction, as demonstrated

(51) Taulelle, F.; Bessada, C.; Massiot, D. *J. Chim. Phys. Phys.−Chim. Biol.* **1992**, *89*, 379.
(52) Engelhardt, G.; Hunger, M.; Koller, H.; Weitkamp, J. *Stud. Surf. Sci. Catal.* **1994**, *84*, 421.
(53) Abragam, A. *Principles of Nuclear Magnetism*; Oxford University Press: London, 1961.
(54) Igarashi, M.; Okubo, N.; Hashimoto, S.; Yoshizaki, R.; Cha, D. J. *Z. Naturforsch., A: Phys. Sci.* **1996**, *51*, 657.
(55) Igarashi, M.; Okubo, N.; Yoshizaki, R. *Z. Naturforsch., A: Phys. Sci.* **1998**, *53*, 442.

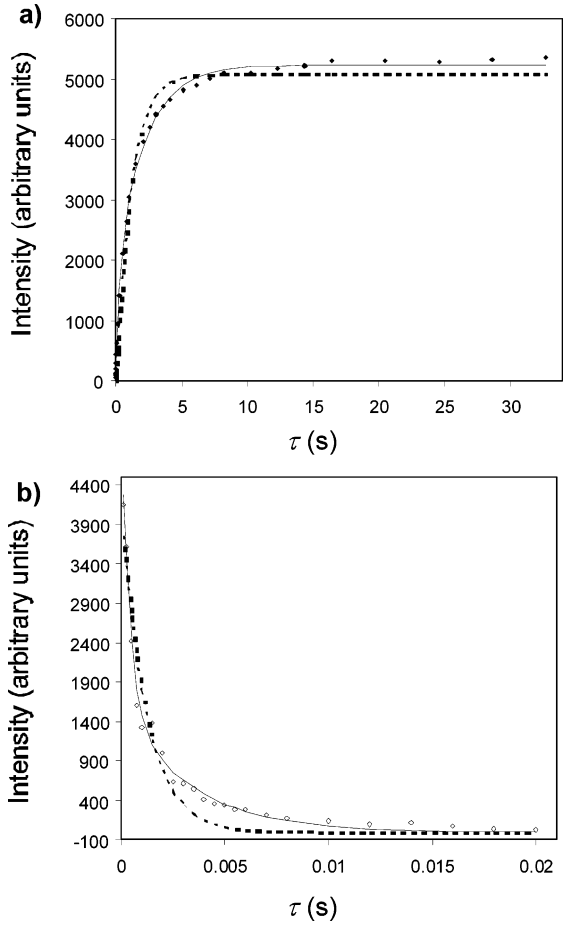

Figure 9. Comparison of monoexponential (dashed lines) and biexponential (solid lines) curve fits for ^{23}Na (a) longitudinal and (b) transverse relaxation data in mesoporous Ti oxides reduced with 1.0 equiv of Na−naphthalene at 22 °C (see Supporting Information for additional data). Errors in the echo intensities are less than 2%.

in the VT NMR experiments above. This and the fact that a biexponential function is necessary to accurately fit the data imply that motion is not in the extreme narrowing limit but on a time scale much slower than that of the ^{23}Na Larmor frequency. The biexponential fits for the channel sodium sites indicate an increased contribution from the "fast" relaxation mechanism as the temperature decreases (e.g., at 100 and −70 °C, the ratios of A_f/A_s are about 0.37 and 1.15, respectively); however, for the framework sites, the ratio of contributions from fast and slow mechanisms do not vary uni-directionally with decreasing temperature. Finally, the longer T_1 of the channel site and smaller changes with decreasing temperature intimate that the channel ions have a relatively high mobility (i.e., less restricted motion) in comparison to those constrained within the mesoporous metal oxide framework.

Measurements of T_2 constants confirm that motion is not in the extreme narrowing limit but rather in the slow motion regime, where T_2's for channel and framework sites are much smaller than T_1's: for instance, in the monoexponential fits, they are on the order of 0.8−1.6 ms and 2.2−7.4 ms, respectively. Once again, biexponential fits provide better agreement with experiment than monoexponential fits (Figure 9b and Supporting Information), though extracted time constants from both are similar. Interestingly, the fits for the channel ions indicate that fast and slow mechanisms make roughly the same contributions at all temperatures, with A_f/A_s between 2.4 and 3.0. However, for the framework ions, an increasing contribution from the "slow" relaxation mechanism is observed with decreasing temperature.

The effective transverse relaxation time constant, T_2^*, can be estimated from $(\pi\Delta\nu_{1/2})^{-1}$, where $\Delta\nu_{1/2}$ is the fwhh obtained from deconvolution of the NMR powder patterns. At room temperature, $\Delta\nu_{1/2} = 300$ Hz and $T_2^* = 1.06$ ms for the channel ions, which is close to the value of 1.19(13) ms obtained monoexponential fits. However, for the framework ions, $\Delta\nu_{1/2} = 2380$ Hz and $T_2^* = 0.14$ ms, which is substantially smaller than the measured T_2 of 3.74(21) ms. This suggests that, for the channel sites, the peak broadening results almost solely from T_2 relaxation, while for the framework sites, the peak broadening results from sources other than transverse relaxation as proposed earlier, that is, a distribution of ^{23}Na quadrupolar interactions.

The only puzzling feature of the transverse relaxation data is that the values of T_2 increase for both the channel and the framework ions as the temperature is decreased. In the slow motion limit of monoexponentially decaying transverse magnetization, one would normally anticipate a decrease in T_2 with decreasing temperature.[56] Biexponential fits do account for the observed behavior, at least for the framework ions, where an increasing contribution from a slow relaxation mechanism is observed. The unusual T_2 constants and increased contribution from a slow relaxation mechanism at low temperatures may be the result of spin diffusion, because the framework Na sites are contained within a fairly flexible mesostructure and may be capable of translational motion through the walls.[56,57]

Lithium-7 NMR. A comparison of the ^{7}Li MAS NMR spectra of the three samples with different reduction levels is shown in Figure 10**.** As the reduction level increases from 0.2 equiv to 1.0 equiv, the single ^{7}Li powder pattern becomes broadened and shifts very slightly in a positive direction (i.e., to the high-frequency direction), with fwhh's of 280, 390, and 650 Hz and centers of gravity at −0.30, −0.20, and +0.14 ppm, for the 0.2 equiv, 0.6 equiv, and 1.0 equiv samples, respectively. Powder patterns corresponding to channel and framework alkali cations are not resolved in the ^{7}Li MAS NMR spectra as they are in the ^{23}Na MAS NMR spectra presented above, and all attempts to deconvolute these peaks into separate broad and narrow resonances were unsuccessful. If there are magnetically distinct Li sites akin to those in the Na-reduced samples, they are likely not resolved because ^{7}Li has a much smaller nuclear quadrupole moment and a reduced chemical shift range (ca. 15−20 ppm) in comparison to ^{23}Na (ca. 40−50 ppm).[50] As a result, relaxation measurements were not conducted. The broadening in the MAS spectra does not arise from ^{7}Li−^{7}Li homonuclear dipolar coupling because the spinning rate of about 8 kHz is enough to average dipolar couplings in most lithium spin

(56) Holcomb, D. F.; Norberg, R. E. *Phys. Rev.* **1955**, *98*, 1074.
(57) Norberg, R. E.; Slichter, C. P. *Phys. Rev.* **1951**, *83*, 1074.

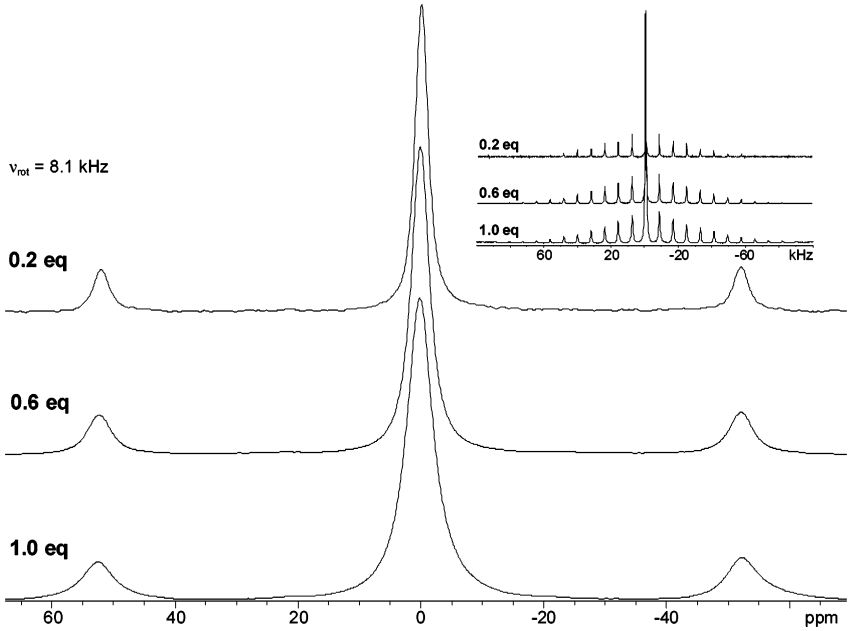

Figure 10. Solid-state ^{7}Li MAS NMR spectra of mesoporous Ti oxide reduced with Li−naphthalene. Inset: full ^{7}Li MAS NMR spectra showing spinning sideband manifolds.

pairs, unless they separated by about 1.3 Å. However, substantial peak broadening is observed in the static ^{7}Li NMR spectra with increased reduction level (Supporting Information), indicating that there is some degree of homonuclear dipolar coupling.

The broadening observed in the MAS spectra likely indicates one of two possibilities: (i) the increasing presence of framework lithium ions or (ii) the gradual creation of a new phase at higher reduction levels. In the first case, the increasing presence of framework Li ions at higher reduction levels would give rise to slightly broader powder patterns, similar to those observed in the ^{23}Na NMR spectra of the Na-reduced samples. The lithium cations which are constrained within the mesoporous Ti oxide framework have a distribution of quadrupolar interactions and chemical shifts and decreased transverse relaxation times, all of which contribute to broadening of the ^{7}Li resonances.[58] In the second case, the subtle chemical shift change from −0.30 to +0.14 ppm in the lithium-reduced mesoporous titanium oxide samples may be due to the presence of local anatase structure with no long-range order at low reduction levels, which is gradually converted to the titanate phase with no long-range order at higher reduction levels. Wagemaker et al. reported three separate lithium chemical shifts in their study of TiO_2 anatase by ^{7}Li MAS NMR.[58] The first peak appearing at −0.85 ppm corresponds to Li intercalated into the anatase structure, the second peak at −2.8 ppm corresponds to Li interacting with the conduction band electrons, and the third peak at 0.7 ppm occurs at high Li reduction levels and corresponds to the formation of lithium titanate. In this study it was also shown that, for increasing lithium concentrations, there is a strong preference for the lithium titanate structure over the anatase phase, which gradually disappears as more and more lithium is added to the host material. Herein, the subtle chemical shift change from −0.30 to +0.14 ppm in the lithium-reduced mesoporous titanium oxide samples may be due to the presence of local anatase structure with no long-range order at low reduction levels, which is gradually converted to the titanate phase with no long-range order at higher reduction levels. Alternatively, the change in the center of gravity of the peak may simply arise from an increased presence of framework Li species possessing a marginally lower chemical shift, as in the case of the ^{23}Na NMR spectra. Unfortunately, the peak width is too broad to make any definitive assignments, and faster MAS speeds or multiple quantum MAS experiments are not helpful in obtaining resolved individual sites.

Conclusions

A series of sodium- and lithium-reduced mesoporous titanium oxide composite materials were synthesized and characterized by nitrogen adsorption, TGA, electrochemical measurements, and XPS. VT conductivity measurements show that these materials are semiconducting. The characterization of guest species in these mesoporous intercalates using solid-state NMR experiments reveals much about the nature of the host material and host−guest interactions. Solid-state ^{23}Na NMR experiments, including VT measurements of T_1 and T_2, reveal that the Na-reduced materials have two distinct Na species: sodium cations which are contained within the large channels and have relatively high mobility and sodium cations which are constrained within the mesoporous framework and have reduced mobility. Unusual transverse relaxation behavior at low temperatures may imply diffusion of framework sodium cations within the walls of the mesoporous structure. Solid-state ^{7}Li NMR experiments on Li-reduced samples reveal only one broad powder pattern which increases in breadth with increased Li impregnation

(58) Wagemaker, M.; van de Krol, R.; Kentgens, A. P. M.; van Well, A. A.; Mulder, F. M. *J. Am. Chem.* Soc. **2001**, *123*, 11454.

that may result from either the increasing presence of framework Li species upon increased reduction, or the gradual conversion from a local Li anatase structure at low reduction to a local Li titanate structure at higher reduction levels.

Acknowledgment. D.M.A. thanks the Petroleum Research Fund administered by the American Chemical Society, as well as the Natural Sciences and Engineering Research Council (NSERC, Canada) and the Ontario Premier's Research Excellence Program for financial support. Dr. M. Stanley Whittingham from SUNY is thanked for his help with electrochemical and TGA measurements. R.W.S. thanks NSERC for research funding in the form of a Discovery Grant, as well as the Canadian Foundation for Innovation (CFI), Ontario Innovation Trust (OIT), and University of Windsor for funding the University of Windsor solid-state NMR laboratories.

Supporting Information Available: Additional longitudinal and transverse relaxation data including mono- and biexponential fits, a table presenting the X^2 values for individual curve fitting, as well as static ^{7}Li NMR spectra of Li-reduced samples. This materials is available free of charge via the Internet at http://pubs.acs.org.

IC051654H